Optical Engineering

OpticalEngineering.SPIEDigitalLibrary.org

Design and fabrication of a miniature objective consisting of high refractive index zinc sulfide lenses for laser surgery

Adam Shadfan
Michal Pawlowski
Ye Wang
Kaushik Subramanian
Ilan Gabay
Adela Ben-Yakar
Tomasz Tkaczyk

SPIE.

Design and fabrication of a miniature objective consisting of high refractive index zinc sulfide lenses for laser surgery

Adam Shadfan,[a] Michal Pawlowski,[a] Ye Wang,[a] Kaushik Subramanian,[b] Ilan Gabay,[b] Adela Ben-Yakar,[b,c] and Tomasz Tkaczyk[a,d,*]

[a]Rice University, Tkaczyk Group, Department of Bioengineering, 6100 Main Street, Houston, Texas 77005, United States
[b]University of Texas at Austin, Ben-Yakar Group, Mechanical Engineering Department, 1 University Station C2200, Austin, Texas 78712, United States
[c]University of Texas at Austin, Ben-Yakar Group, Biomedical Engineering Department, 1 University Station C0800, Austin, Texas 78712, United States
[d]Rice University, Electrical and Computer Engineering Department, 6100 Main Street, Houston, Texas 77005-1892, United States

Abstract. A miniature laser ablation probe relying on an optical fiber to deliver light requires a high coupling efficiency objective with sufficient magnification in order to provide adequate power and field for surgery. A diffraction-limited optical design is presented that utilizes high refractive index zinc sulfide to meet specifications while reducing the miniature objective down to two lenses. The design has a hypercentric conjugate plane on the fiber side and is telecentric on the tissue end. Two versions of the objective were built on a diamond lathe—a traditional cylindrical design and a custom-tapered mount. Both received an antireflective coating. The objectives performed as designed in terms of observable resolution and field of view as measured by imaging a 1951 USAF resolution target. The slanted edge technique was used to find Strehl ratios of 0.75 and 0.78, respectively, indicating nearly diffraction-limited performance. Finally, preliminary ablation experiments indicated threshold fluence of gold film was comparable to similar reported probes.
[DOI: 10.1117/1.OE.55.2.025107]

Keywords: microsurgery; ultrafast laser; optics; optical design; biomedical optics; lasers in medicine.

Paper 151631 received Nov. 19, 2015; accepted for publication Jan. 27, 2016; published online Feb. 23, 2016.

1 Introduction

Laser ablation surgical therapies have been shown to treat a wide array of conditions including endometriosis, epilepsy, thyroid nodules, varicose veins, prostate cancer, and many others.[1–6] While laser ablation can be broadly defined as the removal of material due to the absorption of laser energy, specifically ultrafast pulsed lasers have shown great promise for use in surgical ablation therapy, providing unmatched precision.[7–9] These systems, however, are often limited by the difficulty of delivering light from the large benchtop lasers to the tissue of a patient.[10,11] One solution is to incorporate flexible optical fibers with miniature optics in order to access difficult to reach regions.

Hollow core photonic crystal fibers (HC-PCFs) have been successfully used in endoscopic probes to deliver ultrafast pulses with fluences sufficient for tissue ablation without damaging the fiber.[11,12] The most recent endoscopic probe has combined miniaturized optics with a piezo-scanned PCF to deliver high-repetition rate amplified femtosecond lasers from a compact fiber laser. This surgery probe showed a reduction in the time per cut through the improvement of repetition rate while maintaining a miniature package and delivering enough pulse energies to ablate fixed tissue samples.[11] The availability of larger air core HC-PCFs can potentially enable delivering larger pulse energies. There is a need for a custom miniature objective designed to couple these large core, low NA fibers in order to provide desired focusing conditions for precision surgery.

To improve the efficiency of laser coupling to the tissue and to meet the specifications necessary for surgery, we present the development of a custom designed miniature objective. In this work, we describe the design, fabrication, and validation of this objective to be used as a surgical probe. To simplify the optical design down to two optical components, a high refractive index material was incorporated. This material, zinc sulfide (ZnS), has been used considerably in IR imaging applications[13–16] and successfully incorporated into a miniature objective.[17] To further reduce complexity of the optical system and to relax assembly tolerances, all optical components were manufactured using diamond turning technology, a prototyping method that allows for the production of spherical and aspherical components without an increase of cost and manufacturing time. To provide a distance invariant object field, the lens is telecentric in the sample space. By incorporating a piezo-scanning fiber to deliver the laser radiation responsible for absorption within the tissue, the miniature probe objective was designed to be hypercentric in the image space in order to collect light emitted by the deflecting fiber-optic tip. The objective was thus reduced to two elements to provide $-13\times$ magnification and a 160 μm field of view (FOV), allowing for adequate energy density within the tissue for surgical applications. Two versions were built: a traditional cylindrical miniature objective

*Address all correspondence to: Tomasz Tkaczyk, E-mail: ttkaczyk@rice.edu

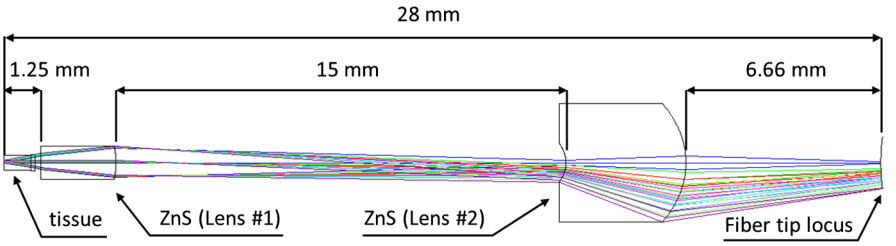

Fig. 1 The optical schematic of the miniature surgery probe.

and a prototype-tapered mount. The optical performance of the tapered objective was characterized by the ablation performance of gold film.

2 Optical System of the Miniature Surgery Probe

The optical design of the distal optics of the surgery probe aims to deliver a sufficiently focused beam of light onto the tissue surface, while the beam is scanned across the back aperture of the optics to achieve the largest possible area of ablation. The optical system of the miniature surgery probe is shown in Fig. 1. The basic optical parameters of the presented system are summarized in Table 1. The optical system was designed in the Zemax (Radiant Zemax, Redmont, Washington) optical design package. At the design state, the system was modeled "in reverse" in order to utilize the built-in Zemax option to launch rays telecentrically in the object space as well as use the optimization operands to target a hypercentric ray configuration at the fiber side of the system.

In Zemax, we constructed the optical system to work with a 10-mm long fiber cantilever. The length of the fiber tip was an important design parameter, as it had direct impact on deflection of the fiber—thus driving the objective aperture requirements. The amplitude of vibration of a fiber cantilever is a function of the electromechanical properties of the piezoelectric tube (PZT, lead zirconium titanate) transducer as well as the elastic properties of the fiber. For the chosen inhibited coupling HC-PCFs (GLOphotonics PMC-PL-780_USP, FRA) and PZT transducer (EBL Products Inc., Connecticut), the 10-mm long fiber cantilever locus of movement forms a sphere with a radius of 6.66 mm. This shape can be achieved when the PZT actuator is activated symmetrically in both the tangential and sagittal planes within the boundaries of its electro-mechanical specification. To replicate this behavior, the image plane of the optical system was modeled as a sphere with a radius of 6.66 mm.

Table 1 Basic optical parameters of the miniature surgery probe.

Tissue side NA	0.23
Magnification	−13×
Design wavelength	770 nm
Tissue side telecentric	Yes
Fiber side hypercentric	Yes
Total length	28 mm
FOV radii (tissue side)	0.08 mm
Fiber deflection	±0.87 mm
Fiber cantilever length	10 mm
Image curvature–fiber side	6.66 mm
Fiber deflection	±2.7 deg

To provide position invariant tissue ablation conditions, energy density at the target must be constant within the field of view. Additionally, for ease of use for the operator of the ablation objective, the whole field of view should be illuminated uniformly. Taking both requirements into account, the optical train of the probe was designed to be telecentric in the tissue space. To avoid self-focusing of laser pulses above the tissue in water and maintain a successful ablation process, we have chosen the beam interrogating the tissue to have an NA of at least 0.2. In order to match the NA of the fiber (0.018) and to guarantee successive ablation, a system with a magnification of −13× was designed that resulted in a tissue side NA of 0.23—above the threshold minimum of 0.2.

To make the surgical probe practical, its outer diameter should be limited to a few millimeters and its length to several centimeters. An appropriate example with similar dimensions to the desired prototype probe is a pen or pencil, which through wide availability and broad use make manipulation of such a probe intuitive. At the early stages of the design, we searched through readily available databases of optical designs like the Zemax Design Library to find optical systems that would meet our size and working conditions constrains but we were unable to match any available design to our requirements. We decided, therefore, to manufacture a custom objective and to simplify the manufacturing and assembly processes by purposefully reducing the count of optical elements down to two. Due to this low count of optical components, we choose to construct our system exclusively from multispectral ZnS in order to decrease aberrational load of each lens. This optical grade crystal has a very high index of refraction ($n = 2.32$ at 770 nm)[18] and can be machined on diamond turning lathes with a root mean squared surface roughness value on the order of a few nanometers.

The design process began with two monochromatic ZnS plane-parallel plates. We set the radii and thicknesses of the optical components as variables. After multiple iterations of optimization of exclusively spherical system, we added the conic variable on subsequent surfaces to widen solutions space for the optimization algorithm. At each step of optimization, the merit function was modified—typically by adding field points and restricting tolerances on the angles of incidence of rays illuminating the fiber tip surface and manually controlling the system magnification and working distance. The optimized final prescription of the optical system of the miniature probe at nominal working conditions is shown in Table 2.

Table 2 Optical prescription data of the miniature surgical probe.

Surface	Radii (mm)	Thickness (mm)	Glass	Semidiameter (mm)	Conic	Comment
1	∞	0.9	Seawater	0.08		Tissue + immersion media
2	∞	0.15	BK7	0.24		Cover glass
3	∞	0.2		0.264		
4	∞	2.5	ZnS	0.312		Lens #1
5	−2.406	15.009		0.559	−1.093	
6	−0.972	4.005	ZnS	0.639	−0.688	Lens #2
7	−2.636	6.5		1.972	−0.628	
8	6.66			0.867		Fiber tip surface

We modeled the superficial layers of tissue combined together with immersion media in Zemax as seawater because the bulk refractive indices of the superficial skin and of the selected immersion media (saline solution) are similar.[19,20] A BK7 cover glass window was used to protect the assembly against accidental scratches and to provide a sealing platform to isolate the optical system from the immersion liquid and other contaminants. Both proximal and distal lenses were made from ZnS and were aspherized in order to achieve diffraction-limited performance in the system with reduced count of active optical surfaces. The optical system was optimized for the following object fields: 0, 0.02, 0.03, 0.038, 0.044, 0.05, 0.06, 0.07, and 0.08 mm located in the tissue space. The corresponding field points in the fiber tip space were located in the tangential plane: 0, 0.23, 0.33, 0.41, 0.47, 0.52, 0.62, 0.73, and 0.85 mm away from the optical axis. The nominal performance metrics of the ablation probe represented by the Fourier transform-based modulation transfer function (MTF) and spot diagrams are shown in Figs. 2(a) and 2(b), respectively.

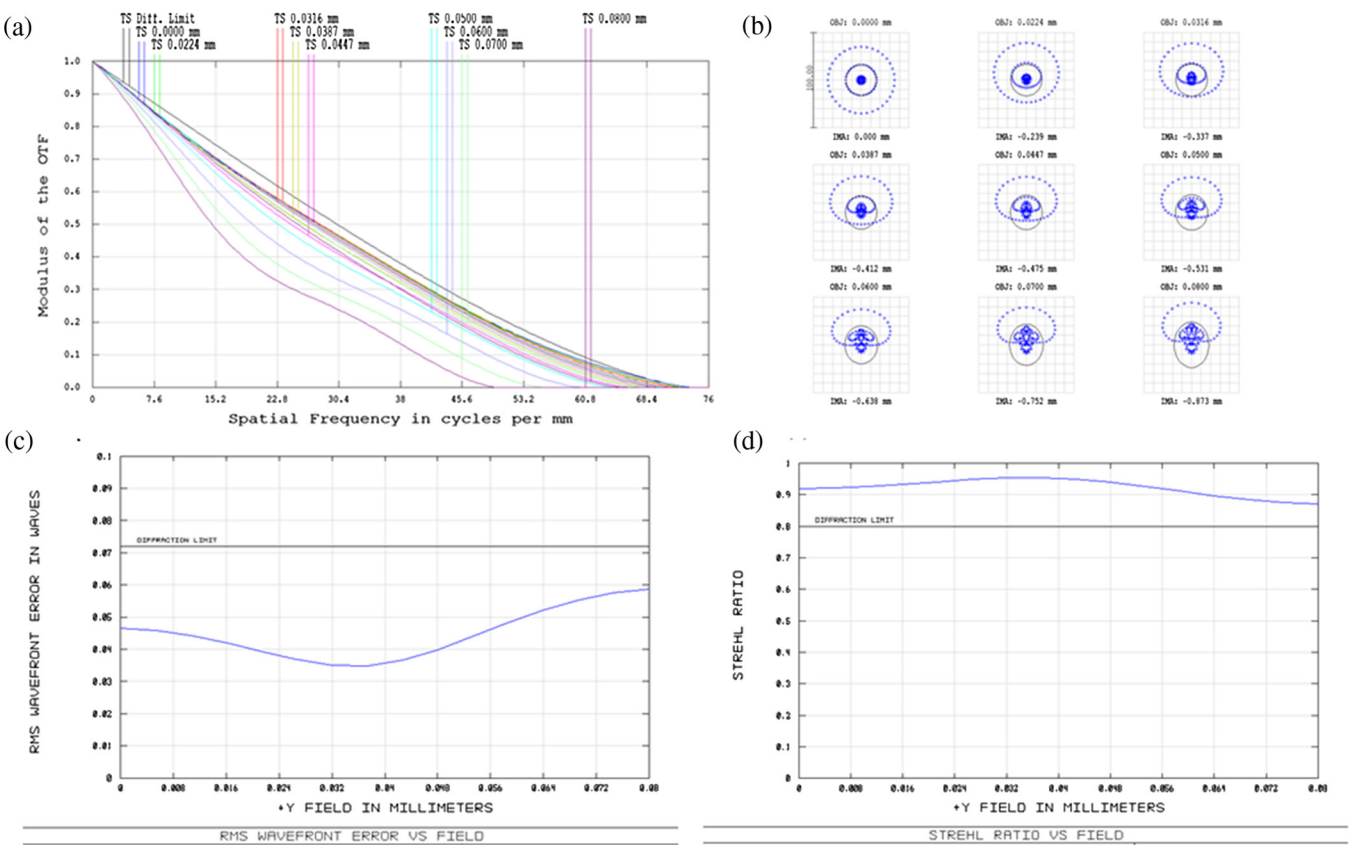

Fig. 2 Nominal performance metrics of the miniature surgical probe: (a) Fourier transform-based MTF and (b) spot diagrams for tangential object points located: 0, 0.02, 0.03, 0.038, 0.044, 0.05, 0.06, 0.07, and 0.08 mm away from the optical axis. The performance is further defined by (c) the RMS wavefront error versus field and (d) the expected SR versus field.

As evidenced by the plots in Fig. 2, the system exhibits diffraction-limited performance within the whole field of view. The performance is further defined in Fig. 2(c) presenting the root mean square (RMS) wavefront error plotted as a function of field and Fig. 2(d) presenting the Strehl ratio (SR) plotted across the field. The SR is a standard relationship that is used to assign a value to the comparison of the measured optical performance to an ideal. Both the expected RMS wavefront error and SR indicate that the design is diffraction limited across the entire field despite the slight drop-off of the MTF curve in Fig. 2(a).

Analysis of the manufacturability of the system was performed in Zemax with the tolerance parameters listed in Table 3. The values of the tolerance operands represent experimentally measured manufacturing capabilities of our machining facility. The performance of the design during tolerance optimization was assessed using root sum square (RSS) and Monte Carlo analysis methods. RMS wavefront error was used in both to indicate system performance. According to the RSS method, the change in performance of the system related to expected manufacturing imperfections will be 0.06. Taking into account the nominal performance of the system (0.045 RMS), an estimate of the prototype RMS error was estimated to be 0.105, a value slightly above diffraction limit of 0.07. Analysis of 999 Monte Carlo simulations runs revealed that there is a 65% chance to manufacture a diffraction-limited system within the whole field of view for tolerances parameters identified in Table 3. Because we planned on manufacturing at least two prototypes, we had a fair chance of producing at least one system that would be diffraction limited or very close to it.

3 Fabrication of Miniature Objective

Due to the differences in sizes of the clear aperture of the two lenses, we investigated constructing an objective that could exploit the variable diameters due to tapering of the probe tip. For this reason, two versions of the objective were manufactured in-house using single point diamond turning (SPDT). A diagram of the two objectives can be seen in Fig. 3, with a traditional design on the left and an experimental-tapered design on the right. The first layout shown in Fig. 3(a), which is similar to many of our previous cylindrical designs,[17,21,22] relies on the inner and outer hypodermic tubes to precisely space and hold the lenses in place. The second lens shown in Fig. 3(b) is a prototype-tapered design that capitalizes on the small clear aperture of the lens closer to the tissue to improve visibility for the operator. The aluminum-tapered mount alone provides all of the mechanical alignment of the two lenses. The tapered region allows for improved visibility of the surgical target while maintaining full-field performance by reducing the external diameter from 5 to 2 mm. The mount was fabricated in the mechanical shop of Rice University.

The production process of the lenses relies on SPDT to both reduce the diameter and cut the surface of optical grade ZnS pellets (Naked Optics, Florida) to the design specifications. SPDT allows for the inclusion of aspherical surfaces, enabling the design to rely on fewer surfaces as conic and higher-order terms may aid in correction of aberrations.[23] For ZnS, we were able to produce high quality optical surfaces, as defined by a surface roughness root mean squared value of 5 nm. The tool path for the cuts of the traditional style objective included flat regions that allows for the internal spacer to be placed precisely without damaging the optically relevant surfaces (clear aperture) of the lenses [as seen in Fig. 3(a)]. For the tapered objective, the lenses were produced in the same fashion as the first design, only requiring a significantly smaller diameter. Two copies of each lens were made in order to improve the probability of producing a diffraction-limited objective. The best lenses were chosen and placed within the mounts. The individual lenses and completed systems can be seen in Fig. 4.

Due to the high refractive index of ZnS, the four optical surfaces of the objective result in a system transmission of only 50.4%, which could prove detrimental for ablation applications by limiting the amount of laser radiation delivered to the tissue. For this reason, the lenses were sent out for

Table 3 Tolerance parameters used during final stage of system optimization. Thickness tolerance for surface 4 was ±0.1 mm.

Radii (mm)	Thickness (mm)	Element tilt (mm)	Surface tilt (mm)	Irregularity (a.u.)	Ref. index (a.u.)
±0.02	±0.02*	±0.02	±0.02	0.2	$\pm 10^{-3}$

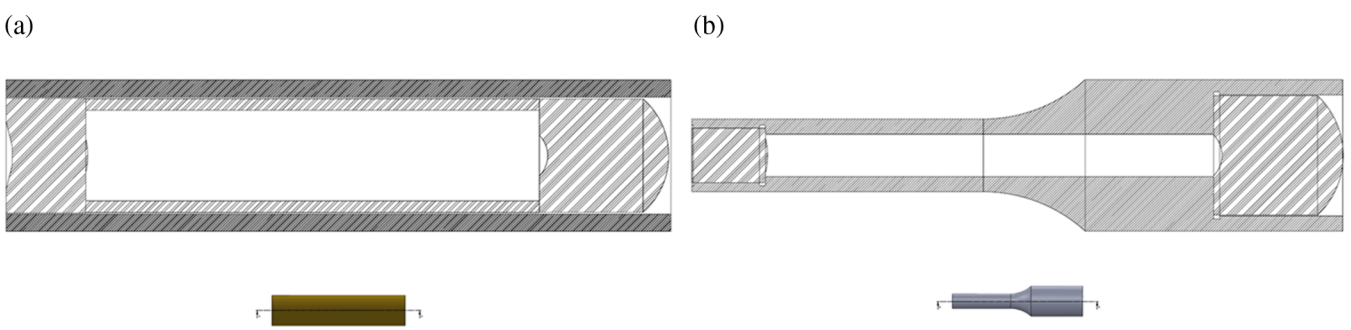

Fig. 3 Mechanical schematic of the two objectives. (a) Traditional design consisting of two ZnS lenses of the same diameter held in place by two hypodermic tubes. (b) Tapered design, using a custom aluminum mount to hold the different sized lenses.

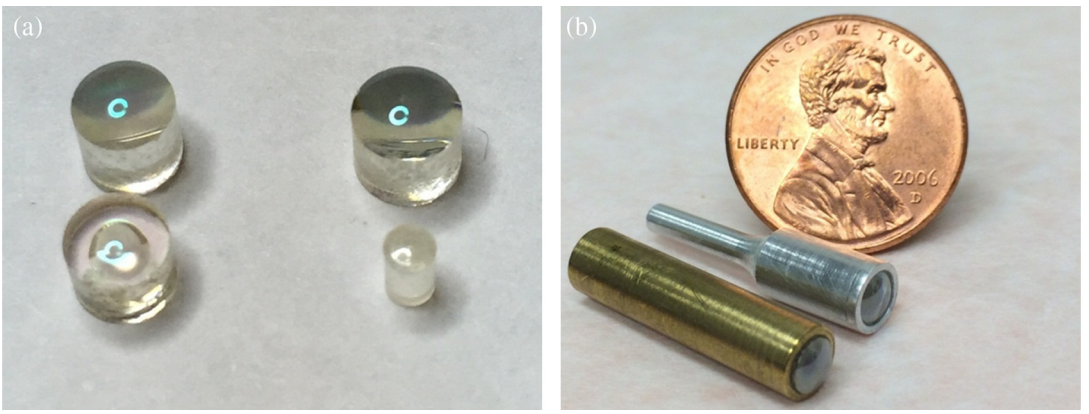

Fig. 4 Pictures of the completed optical components. (a) Completed lenses. Traditional style lenses on the left and the tapered design on the right. (b) Completed versions of both styles of objectives with penny for scale.

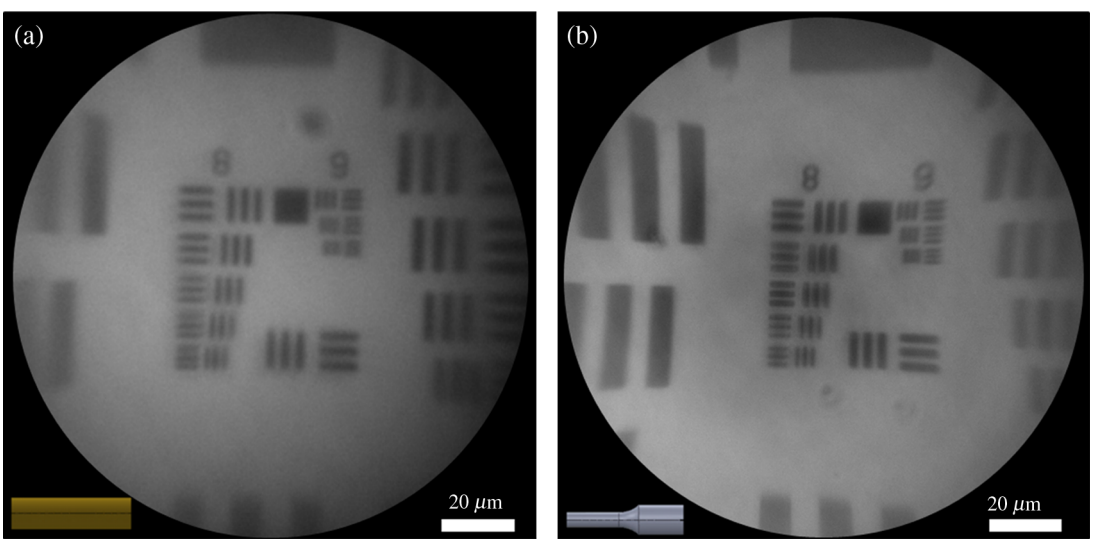

Fig. 5 Comparison of 1951 USAF resolution target imaged by the two objectives before antireflective coatings was applied to (a) the traditional style objective and (b) the tapered objective.

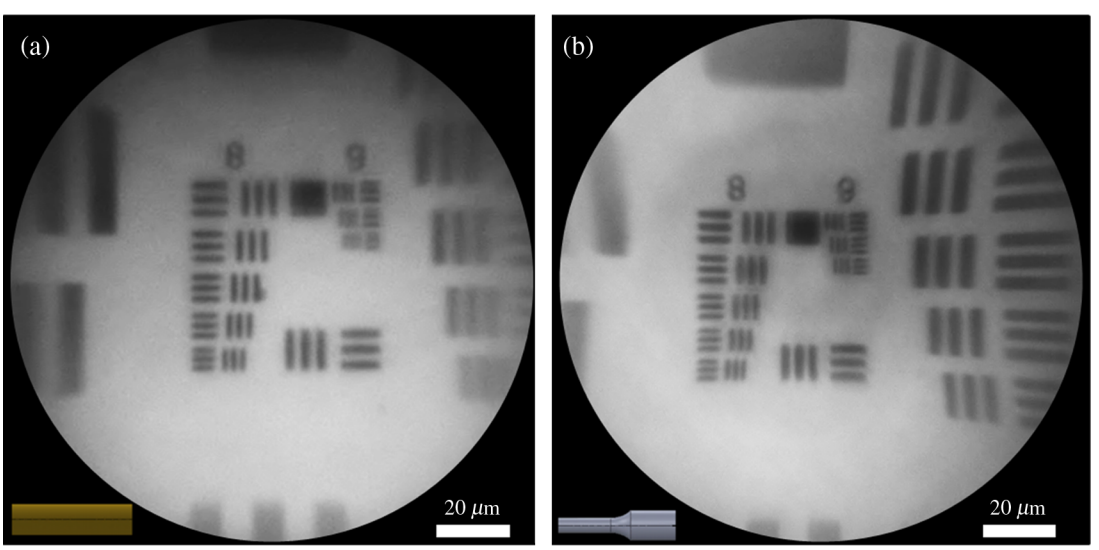

Fig. 6 Comparison of 1951 USAF resolution target imaged by the two objectives after antireflective coatings was applied to (a) the traditional style objective and (b) the tapered objective.

antireflective coatings (Optical Filter Source LLC, Texas). The coatings consisted of a combination of high and low index refractory oxides to provide less than 1% reflectance at the designed 770 nm. The optical performance of the two objectives was observed before and after the coating.

4 Optical Performance of the Two Objectives

To assess the optical performance of the objectives, a 1951 USAF resolution target was imaged. Analysis of the resolution target allows for the estimation of achievable resolution and contrast by calculating the SR. The slanted edge technique is used to approximate the SR by comparing the area under the measured MTF to the theoretical MTF.[24] This comparison was made possible by measuring the contrast between the dark and white regions of the resolution target as imaged by the objective. In general, an SR of 0.8 is considered as diffraction limited.

The optical layout of the testing system consisted of an illumination setup (halogen lamp, 770 nm filter, and focusing optics) and detection optics (the miniature objective, a

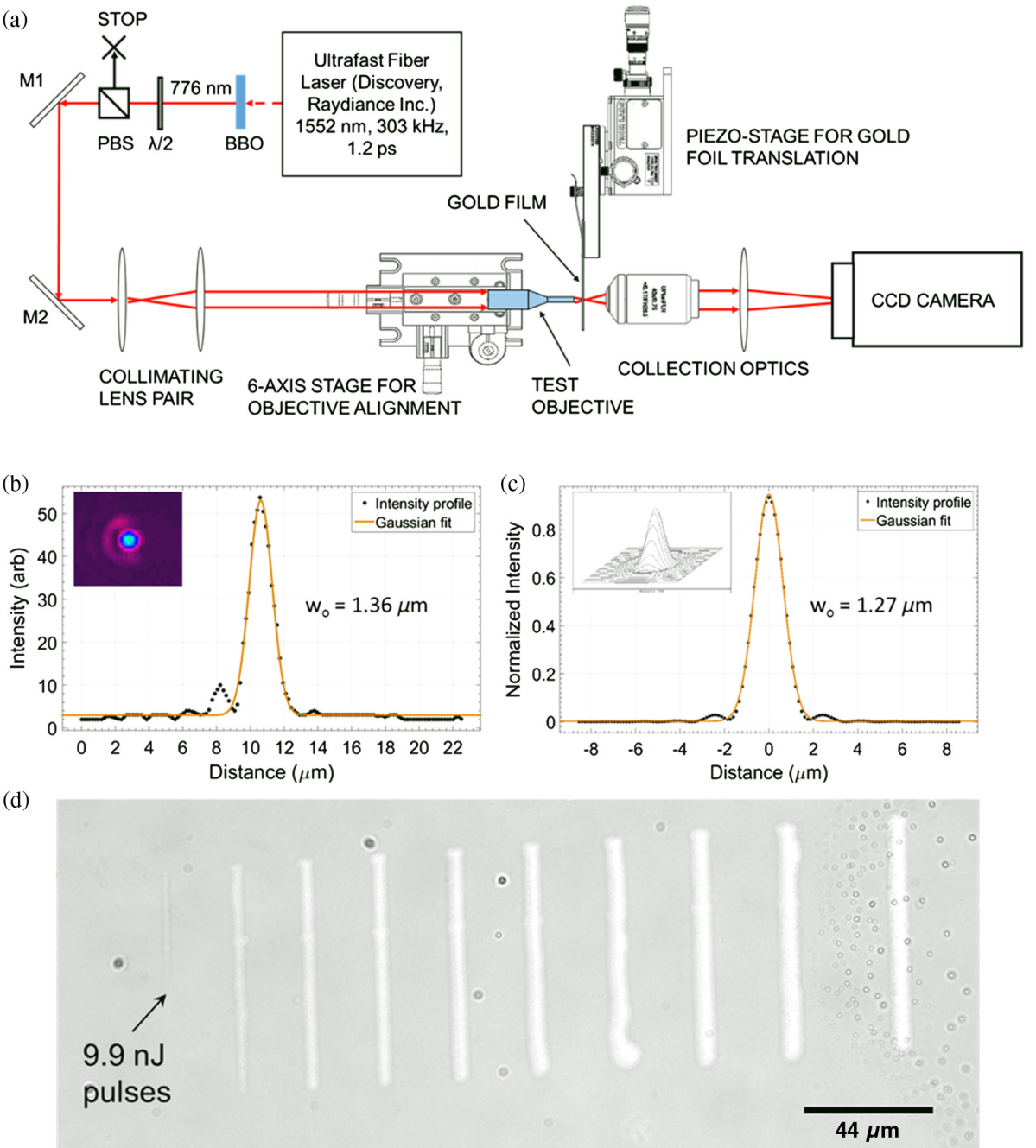

Fig. 7 Spot size characterization and ablation performance of tapered objective. (a) Optical setup for PSF measurements and gold ablation experiments. (b) Measured $1/e^2$ spot size of the coupled laser beam at the focal plane. The inset shows image of the spot size. (c) Theoretical estimate of the $1/e^2$ spot size from the Huygen's point spread function. The inset shows the three-dimensional PSF distribution generated by Zemax. (d) Gold film ablation using the tapered objective at different input laser energies, starting at 9.9 nJ on the left up to 198 nJ on the right.

commercial 0.23NA 10× objective, and a CCD camera). During testing, the custom objective was not water immersed as designed, resulting in a small change in conjugate planes and subsequent magnification (from 13× down to 11×) as calculated using Zemax. At 770 nm, and without water immersion, the expected field of view was 160 μm with an achievable resolution of 2.04 μm according to the Rayleigh criterion. For the resolution target, resolving 2.04 μm corresponds to distinguish at least the individual elements of group 8, element 6. Images of the target through both the traditional style and the tapered objectives before antireflective coating can be seen in Fig. 5.

From Fig. 5, it is apparent that the tapered objective provides improved contrast and resolution over the traditional lenses. The traditional design resolves group 8, element 5 while the tapered design seems capable of resolving group 8, element 6 in agreement with the expected performance. The SRs for the two objectives were 0.55 and 0.65, respectively. In addition to the SR, the full width at half maximum (FWHM) of the line spread function (LSF) was calculated. FWHM averages of 1.23 and 1.15 μm were found for the traditional style objective and the tapered lens, respectively, while the expected value was 1.07 μm. The low SR values were expected due to the low transmission value of ZnS. Again, for this reason, antireflective coatings were applied. Some damage occurred to the optical surfaces of the lenses either during transportation or the coating process. The same resolution target was imaged after coatings and can be seen in Fig. 6.

After coating, both versions showed improvement in contrast as assessed by the increase in SRs up to 0.75 and 0.78, respectively. Additionally, both were able to resolve the expected group 8, element 6, though this improvement may have occurred due to a slight change in alignment of the lenses. There was an expected slight decrease in the FWHM of the LSF (1.14 and 1.12 μm, respectively) in conjunction with the improvement in achievable resolution. In both cases, the objectives were capable of imaging the correct size field of view and expected resolution, and were very close to be diffraction-limited systems as defined by the SR. With objectives performing optically as expected after the antireflective coatings were applied, the enclosures were sealed and ablation experiments began.

5 Ablation Performance

In addition to characterize the imaging resolution, we also characterized the spot size of the laser as focused by the objective. The spot size determines the maximum deliverable fluence by the objective for a given laser input energy and is a critical performance metric for ablation applications. In addition to the focal spot size, the transmission efficiency of the objective for the operating wavelength in the near-infrared is also needed to effectively establish the maximum ablation threshold capabilities of the objective.

To determine the focal spot size of the objective, we aligned a 303 kHz, 776 nm, 1.5 ps laser (Discovery, Raydiance Inc., California) on the back aperture of the tapered objective, which was mounted on a 5-axis stage (Newport Ultralign 561D, California). The optical setup for spot size measurement is shown in Fig. 7(a). The laser beam was collimated and sized to fill the back aperture of the custom objective. The 5-axis stage that the objective was mounted allowed for the alignment of the laser beam along the objective's optic axis. The resultant spot size was imaged onto a CCD beam profiler (UC-680, Uniq Vision, California) using a 40× objective (Olympus UPlanFLN, Japan). A Gaussian function was fit to the intensity profile obtained from the image to determine the focal spot size shown in Fig. 7(b). The measured $1/e^2$ spot size of 1.36 ± 0.07 μm compared well to the Zemax Huygen's point spread function (PSF) estimate for the $1/e^2$ spot size of 1.27 ± 0.02 μm [Fig. 7(c)]. The results showed a near diffraction limit performance for the objective. Next, the transmission efficiency of the objective was measured to be 60% up to 2 μJ of input laser energy showing that the objective maintained linear performance at the operating energy values.

Finally, we proceeded to test the ablation characteristics of the objective. We deposited a thin layer of gold on a cover glass (~15 nm) and placed it at the focal plane of the device. A continuous stream of laser pulses at different pulse energies was allowed to interact with the gold sample as the sample was translated linearly [Fig. 7(d)]. The linear translation speed of the gold slide was adjusted to allow 2 overlapping pulses per each spot. We observed that ablation occurred for all energies above 10 ± 3 nJ, which corresponded to a threshold fluence of 173 ± 58 mJ/cm^2 for gold, and compared well with previously obtained values for gold film thresholds.[25] The maximum fluence deliverable by the objective was 3.4 J/cm^2, sufficient for the designed tissue ablation criterion.

6 Conclusions

Current generation surgical ablation probes suffer from miniaturization and inefficient coupling with a laser. To improve upon these deficiencies, a custom miniature optical surgical objective was designed and fabricated for use in ablation surgery. The design is unique that relies on a hypercentric image space and a telecentric object space to provide −13× magnification of light from a 0.018NA fiber to 0.23NA at the tissue. This design was limited to two lenses by using a high refractive index crystal material (ZnS) and aspheric surfaces. Two variations of the objective were made —a traditional style cylindrical design and a tapered version that reduces the outer diameter while maintaining similar performance. Both variations were coated with antireflecting coatings. While slight damage did occur to the lenses during the antireflective coating process, the optical performance of both objectives was improved to nearly diffraction-limited performance. Finally, the preliminary ablation experimentation compared well with the previously reported values for gold film thresholds by providing a threshold fluence of 173 ± 58 mJ/cm^2.

Acknowledgments

Research reported in this publication was supported by the National Cancer Institute of Biomedical Imaging and Bioengineering under Award No. R21EB015022. The content is solely the responsibility of the authors and does not necessarily represent the official views of the National Institutes of Health. Additionally, this work was supported by the Cancer Prevention and Research Institute of Texas under Award No. RP130412.

References

1. J. P. Daniels et al., "Second generation endometrial ablation techniques for heavy menstrual bleeding: network meta-analysis," *BMJ* **344**, e2564 (2012).
2. Z. Tovar-Spinoza et al., "The use of MRI-guided laser-induced thermal ablation for epilepsy," *Childs Nerv. Syst.* **29**, 2089–2094 (2013).
3. E. Papini et al., "Long-term efficacy of ultrasound-guided laser ablation for benign solid thyroid nodules. Results of a three-year multicenter prospective randomized trial," *J. Clin. Endocrinol. Metab.* **99**, 3653–3659 (2014).
4. S. M. Müllers et al., "Outcome following selective fetoscopic laser ablation for twin to twin transfusion syndrome: an 8 year national collaborative experience," *Eur. J. Obstet. Gynecol. Reprod. Biol.* **191**, 125–129 (2015).
5. K. Kane et al., "The incidence and outcome of endothermal heat-induced thrombosis after endovenous laser ablation," *Ann. Vasc. Surg.* **28**, 1744–1750 (2014).
6. H. Lepor et al., "Complications, recovery, and early functional outcomes and oncologic control following in-bore focal laser ablation of prostate cancer," *Eur. Urol.* **68**, 924–926 (2015).
7. A. H. Hawasli et al., "Stereotactic laser ablation of high-grade gliomas," *Neurosurg. Focus.* **37**, E1 (2014).
8. D. C. Jeong, P. S. Tsai, and D. Kleinfeld, "Prospect for feedback guided surgery with ultra-short pulsed laser light," *Curr. Opin. Neurobiol.* **22**(1), 24–33 (2012).
9. W. Yan et al., "Controllable generation of reactive oxygen species by femtosecond-laser irradiation," *Appl. Phys. Lett.* **104**, 083703 (2014).
10. C. L. Hoy et al., "Clinical ultrafast laser surgery: recent advances and future directions," *IEEE J. Sel. Top. Quantum Electron.* **20**, 242–255 (2014).
11. O. Ferhanoglu et al., "A 5-mm piezo-scanning fiber device for high speed ultrafast laser microsurgery," *Biomed. Opt. Express* **5**, 2023 (2014).
12. C. L. Hoy et al., "Miniaturized probe for femtosecond laser microsurgery and two-photon imaging," *Opt. Express* **16**, 9996–10005 (2008).
13. S. Sparrold et al., "Refractive lens design for simultaneous SWIR and LWIR imaging," *Proc. SPIE* **8012**, 801224 (2011).
14. E. Herman et al., "System design process for refractive simultaneous short and long wave infrared imaging," *Appl. Opt.* **52**, 2761–2772 (2013).
15. P. R. Leite, Jr., M. da Silva, and E. T. Paoli, "Design of an optical system for a 5th generation multi-spectral air-to-air missile considering the imaging performance degradation due to the aerodynamic heating," **7338**, 73380I (2009).
16. Q. An et al., "Mid-infrared waveguides in zinc sulfide crystal," *Opt. Mater. Express* **3**, 466–471 (2013).
17. A. Shadfan et al., "Confocal foveated endomicroscope for the detection of esophageal carcinoma," *Biomed. Opt. Express* **6**, 2311–2324 (2015).
18. M. Debenham, "Refractive indices of zinc sulfide in the 0405 − 13-μm wavelength range," *Appl. Opt.* **23**, 2238–2239 (1984).
19. H. Ding et al., "Refractive indices of human skin tissues at eight wavelengths and estimated dispersion relations between 300 and 1600 nm," *Phys. Med. Biol.* **51**, 1479 (2006).
20. R. M. Pearson, "The refractive index of contact lens saline solutions," *Cont. Lens Anterior Eye* **36**, 136–139 (2013).
21. R. T. Kester et al., "High numerical aperture microendoscope objective for a fiber confocal reflectance microscope," *Opt. Express* **15**, 2409–2420 (2007).
22. M. Kyrish et al., "Ultra-slim plastic endomicroscope objective for nonlinear microscopy," *Opt. Express* **19**, 7603–7615 (2011).
23. T. T. Saito, "Diamond turning of optics," *Opt. Eng.* **15**, 155431 (1976).
24. A. P. Tzannes and J. M. Mooney, "Measurement of the modulation transfer function of infrared cameras," *Opt. Eng.* **34**, 1808 (1995).
25. K. Venkatakrishnan, B. Tan, and B. K. A. Ngoi, "Femtosecond pulsed laser ablation of thin gold film," *Opt. Laser Technol.* **34**, 199–202 (2002).

Adam Shadfan is a PhD candidate in the Biomedical Engineering Department at Rice University. He received his BS degree in biomedical engineering physics from Texas A&M University in 2011. He works in the Tomasz Tkaczyk Optics Lab. His current research interests include optical design, instrumentation, and diagnostics.

Michal Pawlowski received his MSc Eng in applied optics from Warsaw University of Technology in 1997 and received a PhD from the same university in 2002. He was a postdoctoral student at the University of Electro-Communications, Tokyo, between 2003 and 2005. Currently, he works at Rice University as a research scientist. His main interests are applied optics, optical design, and bioengineering.

Ye Wang received her BS degree in physics at Nanjing University in 2013. Currently, she is a third-year PhD student in the applied physics at Rice University and is a research assistant working in the Laboratory of Tomasz Tkaczyk. Her research interests include fiber-based spectroscopy, optical design and fabrication, and biomedical imaging.

Kaushik Subramanian received his MS degree in mechanical engineering from the University of Michigan in 2008. After three years in industry, he is currently pursuing his PhD in mechanical engineering at the University of Texas at Austin under Professor Adela Ben-Yakar. Over the past three years, his research has focused on understanding the interaction of ultrafast pulses with gold nanoparticles suspended in liquid media, and developing endoscopic probes for ultrafast laser delivery for image guided subsurface microsurgery.

Ilan Gabay is currently a postdoctoral research scholar at Professor Ben-Yakar's FemtoLab, at the University of Texas at Austin, leading the research on image-guided, subsurface endoscopic microsurgery. Before that, as a postdoctoral research associate at Professor Capasso's Group at Harvard University, he developed an ultrasensitive fiber-optic spectrometer using a quantum cascade laser for the detection of chemicals in water. As a PhD candidate in Professor Katzir's Applied Physics Group, Tel Aviv University, his research focused on laser tissue bonding.

Adela Ben-Yakar is an associate professor of mechanical and biomedical engineering at the University of Texas at Austin. She received her PhD from Stanford University in 2000 and was a postdoctoral fellow in the Applied Physics Department at Stanford and Harvard Universities from 2000 to 2004. She is an OSA fellow and a recipient of the Fulbright Scholarship, Zonta Amelia Earhart Award, NSF Career Award, Human Frontier Science Program Research Award, and the NIH Director's Transformative Award.

Tomasz Tkaczyk is an associate professor of bioengineering and electrical and computer engineering at Rice University. His research is in microscopy, endoscopy, cost-effective high-performance optics for diagnostics, and snapshot imaging systems. He received his MS and PhD degrees from the Institute of Micromechanics and Photonics, Warsaw University of Technology. In 2003, he began working as a research professor at the College of Optical Sciences, University of Arizona. He joined Rice University in 2007.